Electronic Communication in a Series of Novel Multistep Redox Systems

Kuangbiao Ma,[†] Fabrizia Fabrizi de Biani,[‡] Michael Bolte,[§] Piero Zanello,[‡] and Matthias Wagner*,[†]

Institut für Anorganische Chemie, J.W. Goethe-Universität Frankfurt, Marie-Curie-Strasse 11, D-60439 Frankfurt (Main), Germany, Dipartimento di Chimica dell'Università, Via Aldo Moro, I-53100 Siena, Italy, and Institut für Organische Chemie, J.W. Goethe-Universität Frankfurt, Marie-Curie-Strasse 11, D-60439 Frankfurt (Main), Germany

Received April 10, 2002

The dinuclear ferrocene complexes {[FcBbipy]$_2$O}(PF$_6$)$_2$, **[5](PF$_6$)$_2$**, and {[FcBbipy]$_2$C(H)CN}(PF$_6$)$_2$, **[7](PF$_6$)$_2$**, and the *ansa*-ferrocenes [1,1′-fc(Bbipy)$_2$NC$_6$H$_4$OMe](PF$_6$)$_2$, **[11](PF$_6$)$_2$**, and [1,1′-fc(Bbipy)$_2$NSiMe$_3$](CO$_2$CF$_3$)$_2$, **[13](CO$_2$CF$_3$)$_2$**, have been synthesized and characterized by X-ray crystallography and cyclic voltammetry [Fc = (C$_5$H$_5$)Fe(C$_5$H$_4$); fc = (C$_5$H$_4$)$_2$Fe; bipy = 2,2′-bipyridine]. Electronic communication between the two 2,2′-bipyridylboronium substituents of each compound was observed, suggesting the reduced radical species to be partially delocalized redox intermediates. The degree of electronic interaction is largely independent from the degree of conformational flexibility of the individual molecule. While charge-transfer processes from the electron-rich ferrocene/1,1′-ferrocenylene moieties into empty π-orbitals of the electron-poor 2,2′-bipyridylboronium cations are well apparent in all compounds, no evidence for charge-transfer interactions from the 4-methoxyphenyl substituent to the [Bbipy]$^+$ fragments of **[11](PF$_6$)$_2$** could be detected.

Introduction

Stable multistep redox systems are of great interest in various areas of current research.[1−4] The redox-active units employed consist either of transition metal complexes (e.g., ferrocene) or of organic molecules possessing extended delocalized π-electron systems (e.g., quinone derivatives; *N*-alkyl pyridinium salts).

Our group has recently developed a novel class of highly redox active compounds comprising one (**A**) to four (**C**) 2,2′-bipyridylboronium, [Bbipy]$^+$, cations that are grouped around a ferrocene backbone (Figure 1).[5] The 2,2′-bipyridylboronium substituent is closely related to the strong electron acceptor diquat[6] (**D**, Figure 1), which behaves as a perfectly stable two-step redox system. Consequently, **A**−**C** are able to accept or deliver a maximum of three to nine electrons.

We are now exploring the potential of **A**−**C** as building blocks (i) for the generation of linear polymers or dendritic macromolecules[7] and (ii) for the synthesis of redox-active anion receptors.[8] In this context, the

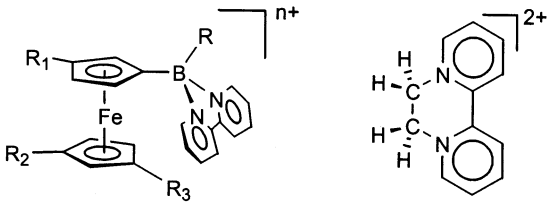

Figure 1.

reaction of the bromo derivative **[1]**$^{2+}$ with water is of particular interest (Scheme 1). Careful hydrolysis of **[1]Br$_2$** with a trace amount of water in the presence of triethylamine and anion exchange with NH$_4$PF$_6$ gave the air- and water-stable *ansa*-ferrocene **[2](PF$_6$)$_2$**.[8] In contrast, treatment of **[1]Br$_2$** with 2.5 equiv of water leads to the open-chain dihydroxy derivative **[3](PF$_6$)$_2$**. Both compounds are dark purple colored, which is likely due to charge-transfer interactions between the electron-rich ferrocene moiety and the electron-poor 2,2′-bipyridylboronium substituents.[5] **[2](PF$_6$)$_2$** is a remarkable compound in several respects: Reduction of the [Bbipy]$^+$ fragments takes place in four well-resolved single-electron processes.[8] Contrary to that, the methyl, methoxy, and dimethyl amino derivatives of **B** (Figure 1) show two reduction waves only, each of them repre-

* Corresponding author. Fax: +49 69 798 29260. E-mail: Matthias.Wagner@chemie.uni-frankfurt.de.
† Institut für Anorganische Chemie, J.W. Goethe-Universität Frankfurt.
‡ Dipartimento di Chimica dell'Università.
§ Institut für Organische Chemie, J.W. Goethe-Universität Frankfurt.

(1) Heck, J.; Dabek, S.; Meyer-Friedrichsen, T.; Wong, H. *Coord. Chem. Rev.* **1999**, *190−192*, 1217.
(2) Ziessel, R.; Hissler, M.; El-ghayoury, A.; Harriman, A. *Coord. Chem. Rev.* **1998**, *178−180*, 1251.
(3) Astruc, D. *Acc. Chem. Res.* **1997**, *30*, 383.
(4) Balzani, V.; Juris, A.; Venturi, M.; Campagna, S.; Serroni, S. *Chem. Rev.* **1996**, *96*, 759.
(5) Fabrizi de Biani, F.; Gmeinwieser, T.; Herdtweck, E.; Jäkle, F.; Laschi, F.; Wagner, M.; Zanello, P. *Organometallics* **1997**, *16*, 4776.
(6) Hünig, S.; Wehner, I. *Heterocycles* **1989**, *28*, 359.
(7) Ding, L.; Ma, K.; Bolte, M.; Fabrizi de Biani, F.; Zanello, P.; Wagner, M. *J. Organomet. Chem.* **2001**, *637−639*, 390.
(8) Ding, L.; Ma, K.; Fabrizi de Biani, F.; Bolte, M.; Zanello, P.; Wagner, M. *Organometallics* **2001**, *20*, 1041.

10.1021/om020284r CCC: $22.00
Publication on Web 08/16/2002

Scheme 1[a]

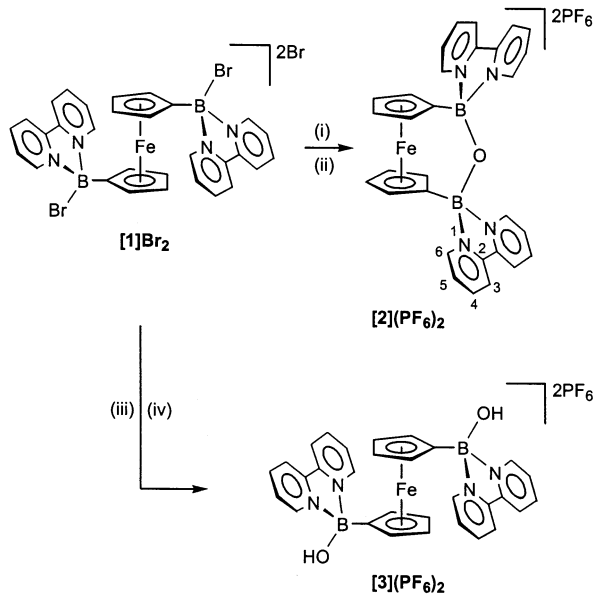

[a] Key: (i) + H_2O/2 NEt_3 (CH_3CN); (ii) + exc. NH_4PF_6 (H_2O); (iii) + exc. H_2O/NEt_3 (CH_3CN); (iv) + exc. NH_4PF_6 (H_2O).

Scheme 2[a]

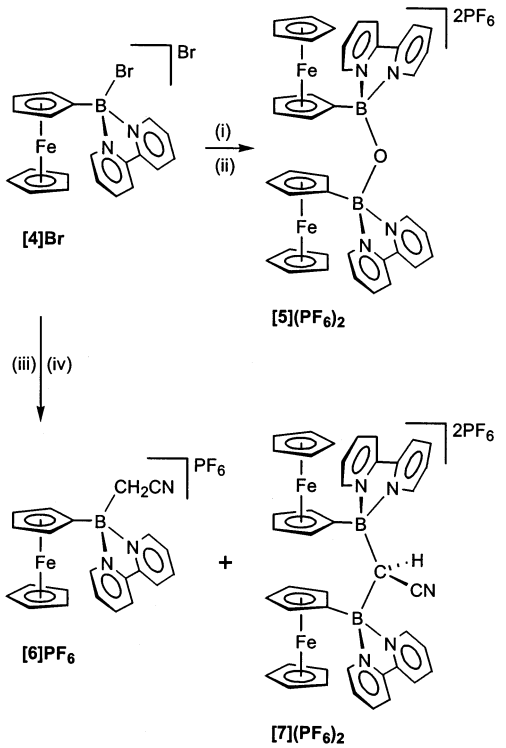

[a] Key: (i) + H_2O/exc. NEt_3 (CH_3CN); (ii) + exc. NH_4PF_6 (H_2O); (iii) + CH_3CN/exc. NEt_3 (CH_3CN); (iv) + exc. NH_4PF_6 (H_2O).

senting a two-electron transition.[5] This leads to the question, whether electronic communication in **[2](PF$_6$)$_2$** is transmitted via the BOB bridge or whether it is merely a Coulomb effect between adjacent redox-active sites.

The crystal structure analysis of **[2](PF$_6$)$_2$** shows the molecule to possess a bowl-shaped cavity, which encapsulates one of the two hexafluorophosphate counteranions.[8] A second question thus arises whether derivatives of **[2](PF$_6$)$_2$** are suitable receptor compounds for the recognition of anionic guest molecules.

Results and Discussion

Syntheses. For a more detailed investigation of the electronic communication between the two bipyridylboronium substituents in **[2](PF$_6$)$_2$**, we decided to synthesize molecules that (i) are closely related to **[2](PF$_6$)$_2$** but possess a higher degree of conformational flexibility and (ii) retain the rigid *ansa*-ferrocene framework but feature bridging atoms other than oxygen. The first class of compounds, which was obtained from the monosubstituted ferrocene **[4]Br**,[5] is represented by the dinuclear BOB-bridged complex **[5](PF$_6$)$_2$** (Scheme 2).

In analogy with the synthesis of **[2](PF$_6$)$_2$**, **[4]Br** was stirred with a trace amount of water in acetonitrile in the presence of excess triethylamine. Anion exchange was achieved by addition of NH_4PF_6 in water to an aqueous solution of **[5]Br$_2$**, whereupon **[5](PF$_6$)$_2$** precipitated quantitatively. As a byproduct of the **[5]Br$_2$** synthesis, we observed the mononuclear species **[6]Br**, which was apparently formed by the deprotonation of solvent molecules and subsequent nucleophilic substitution of the bromo substituent of **[4]Br**. Complex **[6]Br** can be synthesized in high yield by prolonged stirring of **[4]Br** and triethylamine in acetonitrile, which has been rigorously dried. Under these conditions, the reaction proceeds even further to give the BCB-bridged dimer **[7]Br$_2$**. **[7]**$^{2+}$ can easily be separated from **[6]**$^{+}$ by repeated recrystallization of the corresponding hexafluorophosphate salts from acetonitrile. **[7](PF$_6$)$_2$** is of interest in the context of this paper, because it offers the possibility to study the electrochemical behavior of two bipyridylboronium fragments linked by a saturated carbon atom. The comparison of **[5](PF$_6$)$_2$** and **[7](PF$_6$)$_2$** will help to evaluate the contribution of electron lone pairs at the bridging atom to the electronic interaction of both [FcBbipy] subunits [Fc = (C_5H_5)Fe(C_5H_4)].

Replacement of the bridging oxygen atom in **[2](PF$_6$)$_2$** by an isoelectronic NR group appeared to be an attractive goal for several reasons. In the first place, we were interested to see whether this modification will have an effect on the general redox chemistry of the molecule. Moreover, we wanted to explore the possibility of charge-transfer interactions between an electron-rich aromatic substituent R and its electron-poor bipyridylboronium neighbors. As far as the supramolecular chemistry of the BOB-bridged **[2]**$^{2+}$ is concerned, it will be possible to estimate the space inside the molecular cavity and its adaptability to guest molecules of different size by generating BN(R)B-bridged analogues of **[2]**$^{2+}$ and varying the steric demand of the nitrogen substituent R [i.e., R = 4-methoxyphenyl, 4-bromophenyl, trimethylsilyl]. In the first attempt, an acetonitrile solution of **[1]Br$_2$** was treated with 1 equiv of 4-methoxyaniline in the presence of NEt_3. Even though this approach mimics the synthesis of **[2]**$^{2+}$ from **[1]Br$_2$** and H_2O/NEt_3, the target ferrocenophane was not obtained, but NMR spectroscopy gave evidence for the presence of an open-chain species **[8]**$^{2+}$ in the reaction mixture (Scheme 3).

The nature of **[8]Br$_2$** was confirmed by its independent high-yield synthesis from **[1]Br$_2$** with excess

Scheme 3[a]

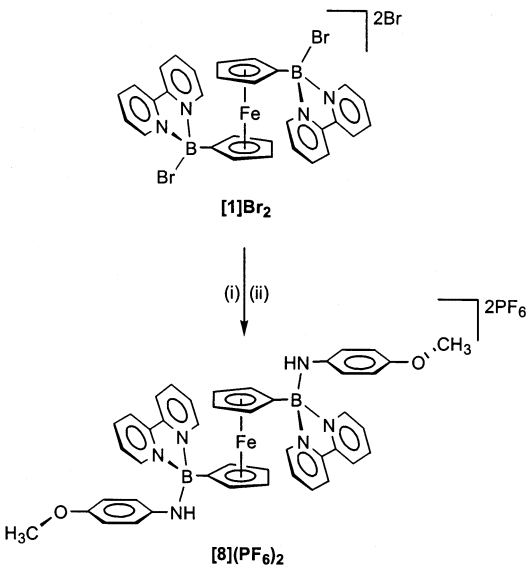

[a] Key: (i) + 4 H_2N-C_6H_4-OMe (CH_2Cl_2); (ii) + exc. NH_4PF_6 (H_2O).

Scheme 4[a]

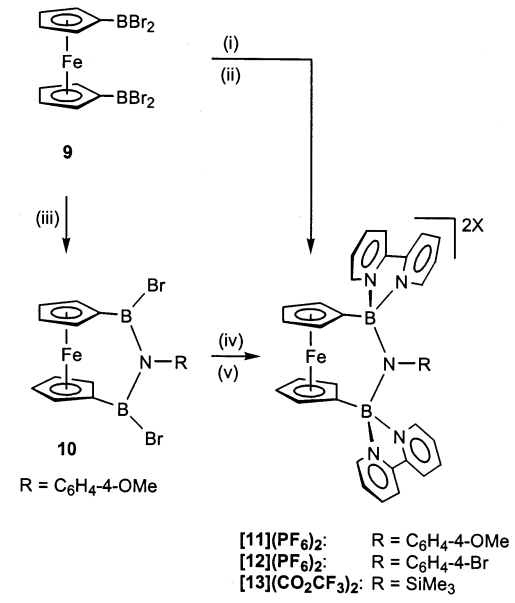

[a] Key: (i) **[12](PF$_6$)$_2$**: + $(Me_3Si)_2N$-C_6H_4-Br (C_7H_8), + 2 bipy (C_7H_8); **[13](Co$_2$CF$_3$)$_2$**: + $LiN(SiMe_3)_2$ (C_7H_8), + 2 bipy (C_7H_8); (ii) **[12](PF$_6$)$_2$**: + 2 $TlPF_6$ (CH_3CN); **[13](Co$_2$CF$_3$)$_2$**: HPLC purification (H_2O/CH_3CN/0.1% HO_2CCF_3); (iii) + H_2N-C_6H_4-OMe/2 NEt_3 (C_7H_8); (iv) + 2 bipy (C_7H_8); (v) + 2 $TlPF_6$ (CH_3CN).

4-methoxyaniline. In the second attempt, we started from **9** and 1 equiv of 4-methoxyaniline/2 equiv of NEt_3 to synthesize the BNB-bridged *ansa*-ferrocene **10** (Scheme 4).[9] Addition of 2 equiv of 2,2′-bipyridine results in the clean formation of **[11]Br$_2$**, which was subsequently transformed into the corresponding hexafluorophosphate salts using $TlPF_6$ in acetonitrile.

The two other derivatives **[12](PF$_6$)$_2$** and **[13](CO$_2$CF$_3$)$_2$** have been obtained from the reaction of **9** with 1 equiv of 4-bromo-*N*,*N*-bis(trimethylsilyl)aniline and lithium bis(trimethylsilyl)amide, respectively, followed by addition of 2 equiv of 2,2′-bipyridine (Scheme 4). In the case of **[12](PF$_6$)$_2$**, anion exchange was again achieved by the addition of $TlPF_6$. In contrast, **[13](CO$_2$CF$_3$)$_2$** crystallized from a sample of **[13]Br$_2$**, which had been purified by HPLC using a mixture of H_2O/0.1% trifluoroacetic acid and acetonitrile (70:30) as eluent.

Spectroscopic Characterization. The NMR spectra of **[3](PF$_6$)$_2$** indicate both [(C_5H_4)B(OH)bipy] fragments to be magnetically equivalent. In CD_3CN, there is no evidence for hindered intramolecular motion due to OH···O hydrogen bonding. All chemical shift values are similar to those reported previously for compound **A** (R = OEt)[5] and therefore do not merit further discussion. The ^{11}B NMR spectrum of **[5](PF$_6$)$_2$** shows one signal at $\delta = 9.2$ typical of tetracoordinated boron nuclei.[10] In the ^{1}H and ^{13}C NMR spectrum, the two ferrocenyl substituents give rise to one set of resonances, which is also true for the bipy fragments and testifies to the high conformational flexibility of the molecule in solution. The general resonance patterns of **[5](PF$_6$)$_2$**, as well as most of the chemical shift values, are rather similar to the NMR data recorded for the *ansa*-bridged analogue **[2](PF$_6$)$_2$**.[8] However, a remarkable upfield shift is observed for the ferrocenyl protons of **[5](PF$_6$)$_2$**, which appear at δ(^{1}H; CD_3CN) = 3.52 (C_5H_5), 3.60, 4.06 (C_5H_4). Contrary to that, the ferrocenyl protons of **[2](PF$_6$)$_2$** are found in the usually observed range [δ(^{1}H; CD_3CN) = 4.30, 4.42 (C_5H_4)]. The NMR spectra of the BCB-bridged dimer **[7](PF$_6$)$_2$** differ from the BOB-bridged counterpart **[5](PF$_6$)$_2$** and from the mononuclear **[6]PF$_6$** in a characteristic way. Now, two sets of ^{1}H and ^{13}C NMR resonances can be distinguished, even when the spectra are run at elevated temperature. This feature is in accordance with the molecular structure suggested for **[7](PF$_6$)$_2$**, which contains a prochiral carbon atom in a central position. Similar to **[5](PF$_6$)$_2$**, the ferrocenyl protons of **[7](PF$_6$)$_2$** experience an upfield shift, which is again most pronounced for the unsubstituted cyclopentadienyl rings [δ(^{1}H; CD_3CN) = 3.37 (C_5H_5)]. In contrast, **[6]PF$_6$** exhibits resonances for the ferrocenyl substituents at δ(^{1}H; CD_3CN) = 4.33, 3.99 (C_5H_4), and 4.12 (C_5H_5). Thus, an individual ferrocenyl moiety in **[5](PF$_6$)$_2$** and **[7](PF$_6$)$_2$** experiences magnetic shielding due to the anisotropy effect of that 2,2′-bipyridylboronium fragment, which is *not* directly attached to it. Integration of the ^{1}H NMR spectrum of **[8](PF$_6$)$_2$** reveals a 1:1 ratio of 4-methoxyphenyl and 2,2′-bipyridyl units in this molecule. All resonances appear in the usually observed shift ranges. The ^{11}B NMR signal of **10** is found at δ(^{11}B; $CDCl_3$) = 46.3. Compared to the starting material 1,1′-fc$(BBr_2)_2$ **9** [δ(^{11}B; C_6D_6) = 50.3],[11] the signal is shifted to higher field by 4 ppm. Compared to the borylamine 1,1′-fc[B(Br)pyr]$_2$ [δ(^{11}B; $CDCl_3$) = 34.4; Hpyr = pyrrolidine],[12] it is less shielded by 11.9 ppm. The ^{11}B NMR spectrum recorded for **10** is thus in agreement with the proposed

(9) Related 1,3-dibora[3]ferrocenophanes have already been described elsewhere: Herberhold, M.; Dörfler, U.; Milius, W.; Wrackmeyer, B. *J. Organomet. Chem.* **1995**, *492*, 59.

(10) Nöth, H.; Wrackmeyer, B. *Nuclear Magnetic Resonance Spectroscopy of Boron Compounds*. In Diehl, P.; Fluck, E.; Kosfeld, R. *NMR Basic Principles and Progress*; Springer: Berlin, 1978; Vol. 14.

(11) Ruf, W.; Renk, T.; Siebert, W. *Z. Naturforsch.* **1976**, *31b*, 1028.

(12) Jäkle, F.; Priermeier, T.; Wagner, M. *Organometallics* **1996**, *15*, 2033.

diborylamine structure. The integrals in the ^{1}H NMR spectrum of **10** reveal a 1:1 ratio between the ferrocenyl backbone (two resonances) and the 4-methoxyphenyl substituent (two resonances), and the number of ^{1}H and ^{13}C NMR signals indicates a high average symmetry of the molecule in solution. Addition of 2,2′-bipyridine to **10** results in a pronounced upfield shift of the ^{11}B NMR resonance, which gives conclusive evidence for the presence of tetracoordinated boron nuclei in the reaction product **[11](PF$_6$)$_2$** [δ(^{11}B; CD_3CN) = 10.0]. Better magnetic shielding is also observed for all protons of the 4-methoxyphenyl substituent in **[11](PF$_6$)$_2$** as compared to **10** {**10**: δ(^{1}H; $CDCl_3$) = 3.86 (OCH_3), 6.95, 7.12 (C_6H_4); **[11](PF$_6$)$_2$**: δ(^{1}H; CD_3CN) = 3.28 (OCH_3), 5.50, 5.90 (C_6H_4)}. Qualitatively similar features are exhibited by the ^{11}B and ^{1}H NMR spectra of the 4-bromophenyl derivative **[12](PF$_6$)$_2$**. It has to be noted in this context that the trimethylsilyl proton signals in **[13](CO$_2$CF$_3$)$_2$** also appear at rather high magnetic field [δ(^{1}H; CD_3CN) = −1.02]. These observations can be attributed to magnetic anisotropy effects caused by the 2,2′-bipyridine units and are in agreement with the assumption that in all three compounds the substituent on the bridging nitrogen atom is residing between the two aromatic bipy planes. Additional structural information stems from the ^{13}C NMR shifts of the 4-methoxyphenyl substituent. In parent 4-methoxyaniline, the carbon atoms in the 2, 3, 5, and 6 position of the aryl ring give rise to signals at δ(^{13}C; $CDCl_3$) = 114.8 and 116.3. These values are shifted to 114.0 and 129.1 ppm in **10** as a result of pronounced N−B π-bonding, which reduces the delocalization of charge from the nitrogen atom into the aryl substituent. Since the boron atoms in **[11](PF$_6$)$_2$** are tetracoordinated, N−B π-bonding is no longer possible. Nevertheless, the ^{13}C NMR data of the 4-methoxyphenyl ring in this compound [δ(^{13}C; CD_3CN) = 114.8, 130.8 for ar-2,3,5,6] deviate significantly from the corresponding resonances of 4-methoxyaniline (see above) and **[8](PF$_6$)$_2$** [δ(^{13}C; CD_3CN) = 115.3, 116.7 for ar-2,3,5,6], but closely resemble those of **10**, indicating that there is no significant N-aryl π-interaction in **[11](PF$_6$)$_2$** as well. This finding can best be explained by assuming a sterically enforced orthogonal conformation between the bridging nitrogen's lone pair and the π-electron cloud of the 4-methoxyphenyl group. The NMR data of the bipy and ferrocene units in **[11](PF$_6$)$_2$**, **[12](PF$_6$)$_2$**, and **[13](CO$_2$CF$_3$)$_2$** resemble each other and those of the BOB-bridged *ansa*-ferrocene **[2](PF$_6$)$_2$**. The UV/vis spectra of the dark purple compounds **[5](PF$_6$)$_2$**, **[7](PF$_6$)$_2$**, **[11](PF$_6$)$_2$**, **[12](PF$_6$)$_2$**, and **[13](CO$_2$CF$_3$)$_2$** exhibit an extremely broad absorption centered at about λ_{max} = 520 nm, which is also common for the open-chain species **A**−**C**.[5] This band has been attributed to charge-transfer processes between the electron-rich ferrocene fragment and its electron-poor diquat-like bipyridylboronium substituents. In the spectrum of **[11](PF$_6$)$_2$**, no significant additional absorptions, which could be assigned to charge-transfer interactions between the 4-methoxyphenyl group and the [Bbipy]$^+$ fragments, are visible in the range of λ = 190−1100 nm.

X-ray Crystal Structure Analyses. The crystallographic data of all compounds under investigation here are summarized in Table 1.

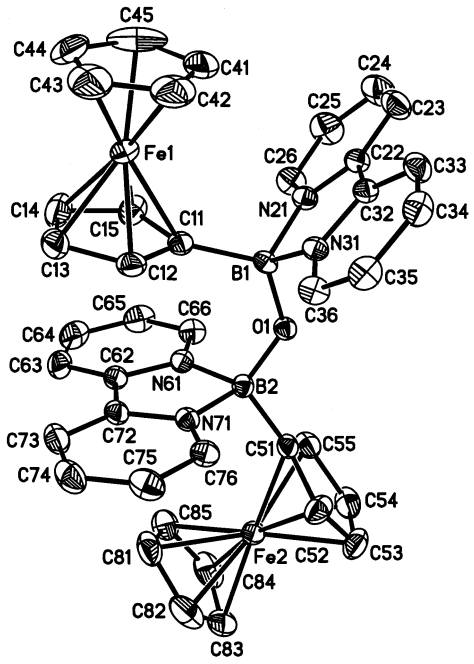

Figure 2. Structure of **[5](PF$_6$)$_2$** in the crystal. Selected bond lengths (Å), angles (deg), and torsion angles (deg); H atoms and $(PF_6)^-$ ions omitted for clarity: B(1)−O(1) = 1.411(2), B(2)−O(1) = 1.412(2), B(1)−C(11) = 1.598(2), B(2)−C(51) = 1.595(2), B(1)−N(21) = 1.628(2), B(1)−N(31) = 1.630(2), B(2)−N(61) = 1.617(2), B(2)−N(71) = 1.619(2); B(1)−O(1)−B(2) = 131.3(1), O(1)−B(1)−C(11) = 119.8(1), O(1)−B(2)−C(51) = 114.1(1), N(21)−B(1)−N(31) = 94.0(1), N(61)−B(2)−N(71) = 94.4(1); C(11)−B(1)−O(1)−B(2) = −1.3(2), B(1)−O(1)−B(2)−C(51) = 178.5(1).

The ferrocene backbone in *ansa*-**[2](PF$_6$)$_2$** enforces a very peculiar conformation of the [(bipy)B−O−B(bipy)] chain with both 2,2′-bipyridine planes pointing into the same direction (see Scheme 1). This results in the formation of a molecular cleft, which harbors one of the two $[PF_6]^-$ counterions.[8] Rotation about the B−O bonds is not restricted in the BOB-bridged dinuclear complex **[5](PF$_6$)$_2$**, in which both 2,2′-bipy ligands are pointing in different directions (Figure 2). The molecule can be divided into two fragments (i.e., Fc1−B(1)bipy and Fc2−B(2)bipy). In both fragments, the 2,2′-bipyridine group adopts a *side-on* conformation with respect to the attached ferrocenyl substituent, which leads to short Fe···bipy through-space distances [Fe(1)···COG1 = 3.718 Å, Fe(2)···COG2 = 3.629 Å; COG1, center of gravity of the B(1)N(21)C(22)C(32)N(31) ring; COG2, center of gravity of the B(2)N(61)C(62)C(72)N(71) ring]. A similar structural motif has been observed in the case of the disubstituted ferrocene **B**.[5] Most interestingly, the Cp ring C(11)C(12)C(13)C(14)C(15) is placed in a position almost parallel to the plane of the B(2)bipy unit (angle between planes C(11)C(12)C(13)C(14)C(15)//B(2)N(61)-C(62)C(72)N(71) = 12.4°; distance between the center of gravity of the C(11)C(12)C(13)C(14)C(15) plane and the midpoint of the C62−C72 bond = 3.26 Å). The boron−oxygen bonds in the dinuclear species **[5](PF$_6$)$_2$** [B(1)−O(1) = 1.411(2) Å; B(2)−O(1) = 1.412(2) Å] possess the same value and are only slightly longer than the corresponding bonds in the *ansa*-derivative **[2](PF$_6$)$_2$** [B(1)−O(1) = 1.398(3) Å; B(2)−O(1) = 1.389(3) Å].[8] The angles around the oxygen atom are rather similar in both compounds {**[5](PF$_6$)$_2$**, B(1)−O(1)−B(2)

Table 1. Crystal Data and Structure Refinement Details for [3](PF$_6$)$_2$, [5](PF$_6$)$_2$, [7](PF$_6$)$_2$, [8](PF$_6$)$_2$, [11](PF$_6$)$_2$, and [13](Co$_2$CF$_3$)$_2$

	[3](PF$_6$)$_2$	[5](PF$_6$)$_2$	[7](PF$_6$)$_2$
formula	$C_{30}H_{26}B_2F_{12}FeN_4O_2P_2$	$C_{40}H_{34}B_2F_{12}Fe_2N_4OP_2$	$C_{46}H_{45}B_2F_{12}Fe_2N_5OP_2$
fw	841.96	1009.97	1107.03
color, shape	red, plate	black, block	brown, needle
temp (K)	173	173	100
radiation	Mo Kα, 0.71073 Å	Mo Kα, 0.71073 Å	Mo Kα, 0.71073 Å
cryst syst	triclinic	monoclinic	monoclinic
space group	$P\bar{1}$	$P2_1/n$	$C2/c$
a (Å)	8.562(2)	14.474(1)	28.385(4)
b (Å)	9.563(2)	20.416(2)	8.210(1)
c (Å)	22.721(4)	14.506(1)	39.339(6)
α (deg)	94.01(1)	90	90
β (deg)	99.32(1)	109.29(1)	93.34(1)
γ (deg)	114.03(1)	90	90
V (Å^3)	1657.6(6)	4046.0(6)	9152.0(20)
Z	2	4	8
D_{calcd} (g cm^{-3})	1.687	1.658	1.607
μ (mm^{-1})	0.657	0.892	0.779
cryst size (mm)	0.22 × 0.18 × 0.06	0.62 × 0.58 × 0.24	0.48 × 0.03 × 0.03
no. of reflns collected	16 841	96 799	46 085
no. of indep reflns	5607	12 154	8237
R(int)	0.0993	0.0286	0.2214
no. of data/restraints/params	5607/0/480	12 154/0/568	8237/10/611
GOF	1.080	1.009	1.034
R1, wR2 ($I>2\sigma(I)$)	0.1127, 0.2509	0.0387, 0.0883	0.1442, 0.2987
R1, wR2 (all data)	0.2021, 0.2977	0.0546, 0.0975	0.2661, 0.3605
largest diff peak and hole (e Å^{-3})	1.608, −0.509	0.669, −0.649	0.485, −0.911

	[8](PF$_6$)$_2$	[11](PF$_6$)$_2$	[13](CO$_2$CF$_3$)$_2$
formula	$C_{44}H_{40}B_2F_{12}FeN_6O_2P_2$	$C_{45}H_{47}B_2F_{12}FeN_7O_2P_2$	$C_{37}H_{33}B_2F_6FeN_5O_4Si$
fw	1052.23	1085.31	831.24
color, shape	violet, plate	violet, plate	violet, plate
temp (K)	146	100	173
radiation	Mo Kα, 0.71073 Å	Mo Kα, 0.71073 Å	Mo Kα, 0.71073 Å
cryst syst	triclinic	triclinic	triclinic
space group	$P\bar{1}$	$P\bar{1}$	$P\bar{1}$
a (Å)	8.874(2)	10.625(2)	10.437(1)
b (Å)	10.652(1)	13.657(3)	11.964(1)
c (Å)	12.752(2)	18.456(4)	15.478(2)
α (deg)	78.98(1)	70.39(1)	84.98(1)
β (deg)	70.69(1)	81.34(2)	87.98(1)
γ (deg)	73.03(1)	69.83(1)	85.22(1)
V (Å^3)	1082.1(3)	2366.2(9)	1917.9(3)
Z	1	2	2
D_{calcd} (g cm^{-3})	1.615	1.523	1.439
μ (mm^{-1})	0.523	0.481	0.500
cryst size (mm)	1.00 × 0.32 × 0.18	0.22 × 0.18 × 0.05	0.48 × 0.46 × 0.10
no. of reflns collected	20 372	16 950	26 440
no. of indep reflns	6643	7996	9835
R(int)	0.0201	0.1152	0.0673
no. of data/restraints/params	6643/0/394	7996/3/627	9835/0/505
GOF	1.543	0.711	1.051
R1, wR2 ($I>2\sigma(I)$)	0.0335, 0.0914	0.0849, 0.1746	0.0731, 0.2109
R1, wR2 (all data)	0.0426, 0.0943	0.2450, 0.2614	0.0886, 0.2189
largest diff peak and hole (e Å^{-3})	0.460, −0.389	0.876, −0.609	0.907, −0.678

= 131.3(1)°; **[2](PF$_6$)$_2$**, B(1)−O(1)−B(2) = 136.2(2)°}, testifying to the fact that the ferrocene backbone imposes only little strain on the BOB linker of **[2](PF$_6$)$_2$**.

The carbon-bridged dinuclear ferrocene complex **[7](PF$_6$)$_2$** exhibits a different conformation in the solid state than its oxygen-bridged counterpart **[5](PF$_6$)$_2$** (Figure 3). Similar to **[2](PF$_6$)$_2$**, both 2,2′-bipyridine ligands are located at the same side of the molecule. However, a "V" shape is observed for the [(bipy)B−C(H)-CN−B(bipy)] moiety in **[7](PF$_6$)$_2$**, while the [(bipy)B−O−B(bipy)] bridge in **[2](PF$_6$)$_2$** is best described as possessing a "W" shape.[8] As a consequence, different angles between the bipy planes are observed in **[2](PF$_6$)$_2$** (73.5°) and **[7](PF$_6$)$_2$** (16.6°). In **[7](PF$_6$)$_2$**, the centers of gravity of the B(1)N(21)C(22)C(32)N(31) ring and the B(2)N(61)C(62)C(72)N(71) plane are only 3.29 Å apart from each other. The boron−carbon bond lengths within the *ansa*-bridge are 1.66(2) Å [B(1)−C(1)] and 1.67(2) Å [B(2)−C(1)] and thus do not deviate appreciably from the value found in the mononuclear species **[6]PF$_6$** [B(1)−C(1) = 1.626(6) Å]. The central B−C−B angle [B(1)−C(1)−B(2) = 124.3(11)°] is stretched by 15° compared to the value of an ideal tetrahedral angle (109.3°). The substructures of the Fc1−B(1)bipy and Fc2−B(2)bipy fragments are almost identical to each other and to the corresponding fragments in **[5](PF$_6$)$_2$** and thus do not merit further discussion.

The hydroxy derivative **[3](PF$_6$)$_2$** features a hydrogen bond between the two oxygen atoms in the solid state (Figure 4). The molecule can thus be regarded as a ferrocenophane possessing a very weak *ansa*-bridge

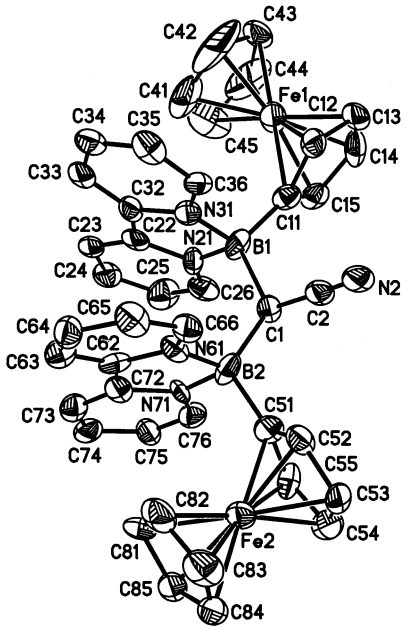

Figure 3. Structure of **[7](PF$_6$)$_2$** in the crystal. Selected bond lengths (Å), angles (deg), and torsion angles (deg); H atoms and $(PF_6)^-$ ions omitted for clarity: B(1)−C(1) = 1.66(2), B(2)−C(1) = 1.67(2), B(1)−C(11) = 1.58(2), B(2)−C(51) = 1.59(2), B(1)−N(21) = 1.57(2), B(1)−N(31) = 1.58(2), B(2)−N(61) = 1.62(2), B(2)−N(71) = 1.60(2), C(1)−C(2) = 1.47(2), C(2)−N(2) = 1.12(2); B(1)−C(1)−B(2) = 124.3(11), C(1)−B(1)−C(11) = 113.5(12), C(1)−B(2)−C(51) = 115.7(12), N(21)−B(1)−N(31) = 97.8(11), N(61)−B(2)−N(71) = 97.8(11), C(2)−C(1)−B(1) = 108.2(12), C(2)−C(1)−B(2) = 107.3(11); C(11)−B(1)−C(1)−B(2) = 177.6(14), C(51)−B(2)−C(1)−B(1) = −178.8(14).

[O(1)−H(1) = 0.84 Å, O(2)···H(1) = 2.36 Å]. The B−O bond lengths [B(1)−O(1) = 1.395(13) Å, B(2)−O(2) = 1.411(14) Å] are not much different from those observed for **[2](PF$_6$)$_2$** and **[5](PF$_6$)$_2$**.

The open-chain derivative **[8](PF$_6$)$_2$** adopts a centrosymmetric structure in the solid state (Figure 5). Its exocyclic boron−nitrogen bond [B(1)−N(1) = 1.469(2) Å] is shorter than the boron−nitrogen bonds within the 2,2′-bipyridylboronium fragment [B(1)−N(21) = 1.616(2) Å, B(1)−N(31) = 1.621(2) Å]. This can be attributed to the fact that coordination of the small boron atom leads to bending of the bipyridyl backbone. The resulting molecular strain is reduced when the B−N bonds are elongated. Two BNB-*ansa*-ferrocenes, **[11](PF$_6$)$_2$** and **[13](CO$_2$CF$_3$)$_2$**, have been characterized by X-ray crystallography. In the case of **[11](PF$_6$)$_2$**, a planar 4-methoxyphenyl group is attached to the nitrogen atom (Figure 6). This substituent is well-suited to minimize short intramolecular contacts and possesses an electron-rich π-system. **[13](CO$_2$CF$_3$)$_2$** bears a sterically demanding trimethylsilyl substituent, which can be expected to exert a positive inductive effect on the BNB bridge (Figure 7). The N-aryl bond in **[11](PF$_6$)$_2$** [N(1)−C(71) = 1.461(12) Å] is significantly longer than the corresponding bonds in **[8](PF$_6$)$_2$** [N(1)−C(41) = 1.409(2) Å]. As has already been deduced from the ^{13}C NMR data of **[11](PF$_6$)$_2$**, an orthogonal conformation is found between the electron lone pair on the bridging nitrogen atom and the aromatic 4-methoxyphenyl substituent [torsion angle: B(2)−N(1)−C(71)−C(72) = 84.9(12)°]. The crystal structure analysis of **[11](PF$_6$)$_2$** thus allows

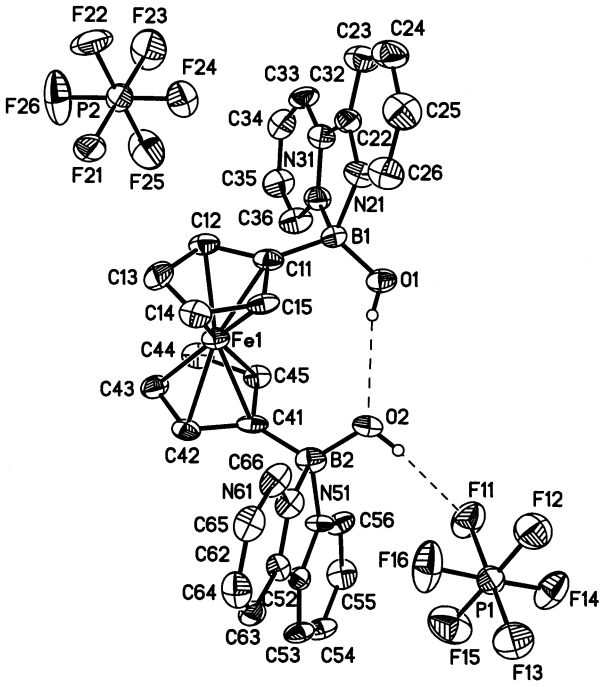

Figure 4. Structure of **[3](PF$_6$)$_2$** in the crystal. Selected bond lengths (Å), angles (deg), and torsion angles (deg); most H atoms omitted for clarity: B(1)−O(1) = 1.395(13), B(2)−O(2) = 1.411(14), B(1)−N(21) = 1.632(15), B(1)−N(31) = 1.600(16), B(2)−N(51) = 1.643(14), B(2)−N(61) = 1.626(14), B(1)−C(11) = 1.590(15), B(2)−C(41) = 1.552(16); C(11)−B(1)−O(1) = 119.1(10), C(41)−B(2)−O(2) = 116.4(10), N(21)−B(1)−N(31) = 94.2(8), N(51)−B(2)−N(61) = 92.9(8), O(1)−B(1)−C(11)−C(15) = 42.4(16), O(2)−B(2)−C(41)−C(45) = 36.8(15), N(21)−B(1)−C(11)−C(12) = 94.3(12), N(51)−B(2)−C(41)−C(42) = 87.0(13). Hydrogen bonds: O(1)−H(1) = 0.84, O(2)···H(1) = 2.36, distance between O(1) and O(2): 3.144(10), O(1)−H(1)···O(2) = 156.0; O(2)−H(2) = 0.84, F(11)···H(2) = 2.09, distance between O(2) and F(11): 2.915(9), O(2)−H(2)···F(11) = 169.1.

us to determine the length of a genuine σ-bond between an sp^2-hybridized nitrogen atom and an sp^2-hybridized carbon atom. The B−N bond lengths in the *ansa*-bridges of **[11](PF$_6$)$_2$** [B(1)−N(1) = 1.485(15) Å, B(2)−N(1) = 1.501(13) Å] and **[13](CO$_2$CF$_3$)$_2$** [B(1)−N(1) = 1.503(5) Å, B(2)−N(1) = 1.503(5) Å] are identical within experimental error. However, the B(1)−N(1)−B(2) angle is larger by 6.8° in **[11](PF$_6$)$_2$** [130.7(8)°] compared to **[13](CO$_2$CF$_3$)$_2$** [123.9(3)°]. Apart from that, the bulky trimethylsilyl group of **[13](CO$_2$CF$_3$)$_2$** apparently has little influence on the overall geometry of the molecular framework. For example, very similar dihedral angles between the two cyclopentadienyl rings are found in **[11](PF$_6$)$_2$** (9.1°) and **[13](CO$_2$CF$_3$)$_2$** (11.3°). The [B(bipy)−N(R)−B(bipy)] bridges thus appear to fit nicely to the structural requirements of the ferrocene backbone [R = 4-methoxyphenyl, SiMe$_3$]. In both ferrocenophanes, the nitrogen atom N(1) has a planar configuration [sum of angles around N(1): 360°]. The N(1)−B(1)−C(11) angles, as well as the N(1)−B(2)−C(41) angles, deviate from the ideal value (109.3°) expected for tetracoordinated boron centers {**[11](PF$_6$)$_2$**, 121.0(9), 119.5(10); **[13](CO$_2$CF$_3$)$_2$**, 123.5(3)°, 122.8(3)°}. In **[11](PF$_6$)$_2$**, the dihedral angle between the B(1)N(31)C(32)C(22)N(21) [B(2)N(61)C(62)C(72)N(71)] plane and the aromatic ring of the 4-methoxyphenyl substituent is 52.7° [58.1°].

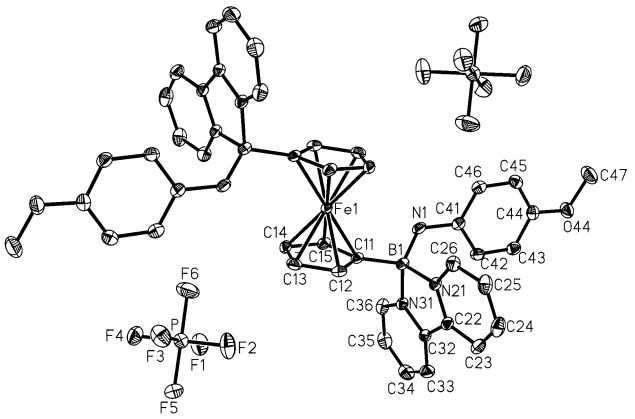

Figure 5. Structure of **[8](PF$_6$)$_2$** in the crystal. Selected bond lengths (Å), angles (deg), and torsion angles (deg); H atoms omitted for clarity: B(1)−N(1) = 1.469(2), B(1)−C(11) = 1.582(2), B(1)−N(21) = 1.616(2), B(1)−N(31) = 1.621(2), N(1)−C(41) = 1.409(2), O(44)−C(44) 1.372(2); N(1)−B(1)−C(11) = 115.2(1), N(21)−B(1)−N(31) = 93.7-(1); B(1)−N(1)−C(41) = 127.2(1), C(11)−B(1)−N(1)−C(41) = 173.2(1), C(15)−C(11)−B(1)−N(1) = 51.4(2), B(1)−N(1)−C(41)−C(42) = 43.9(2), C(45)−C(44)−O(44)−C(47) = 6.6(2).

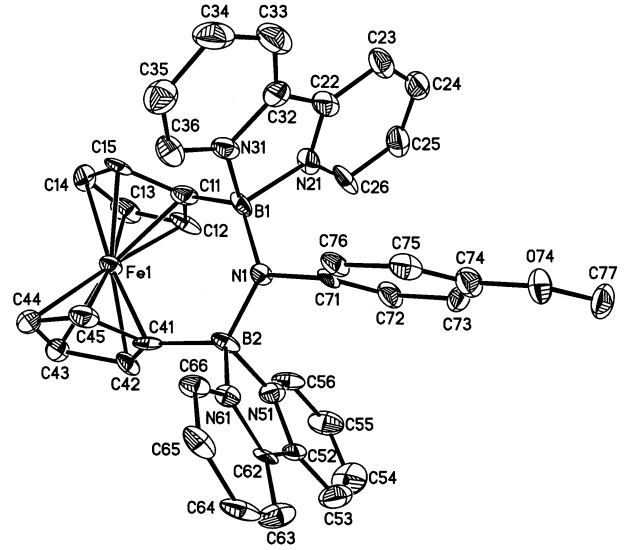

Figure 6. Structure of **[11](PF$_6$)$_2$** in the crystal. Selected bond lengths (Å), angles (deg), and torsion angles (deg); H atoms and $(PF_6)^-$ ions omitted for clarity: B(1)−N(1) = 1.485(15), B(2)−N(1) = 1.501(13), B(1)−N(21) = 1.636(13), B(1)−N(31) = 1.658(14), B(2)−N(51) = 1.639(15), B(2)−N(61) = 1.639(14), B(1)−C(11) = 1.569(16), B(2)−C(41) = 1.608(16), N(1)−C(71) = 1.461(12), O(74)−C(74) = 1.390(13); B(1)−N(1)−B(2) = 130.7(8), B(1)−N(1)−C(71) = 115.1(8), B(2)−N(1)−C(71) = 114.2(9), N(1)−B(1)−C(11) = 121.0(9), N(1)−B(2)−C(41) = 119.5(10), N(21)−B(1)−N(31) = 92.6(7), N(51)−B(2)−N(61) = 94.7(8); C(11)−B(1)−N(1)−B(2) = −12.9(16), C(41)−B(2)−N(1)−B(1) = −13.7(16); C(11)−B(1)−N(1)−C(71) = 168.1(9), C(41)−B(2)−N(1)−C(71) = 165.3(8), B(1)−N(1)−C(71)−C(76) = 82.5(12), B(2)−N(1)−C(71)−C(72) = 84.9(12), C(77)−O(74)−C(74)−C(73) = 7.4(16); C(11)−C(15)//C(41)−C(45) = 9.1.

Electrochemistry. Similar to the previously reported complex **[2]**$^{2+}$,[8] dications **[11]**$^{2+}$−**[13]**$^{2+}$ undergo a ferrocene-centered oxidation and two doubly split bipy-centered reductions. All these processes display features of chemical reversibility on the cyclic voltammetric time scale. As a typical example, Figure 8 compares the cyclic

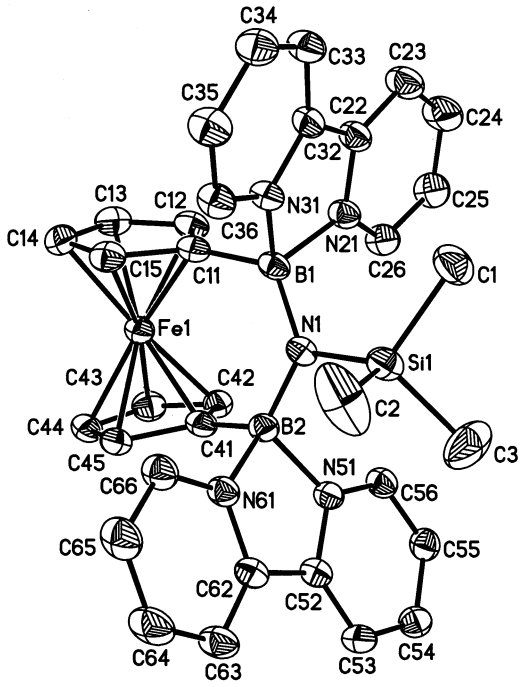

Figure 7. Structure of **[13](CO$_2$CF$_3$)$_2$** in the crystal. Selected bond lengths (Å), angles (deg), and torsion angles (deg); H atoms and $(CO_2CF_3)^-$ ions omitted for clarity: B(1)−N(1) = 1.503(5), B(2)−N(1) = 1.503(5), B(1)−N(21) = 1.633(5), B(1)−N(31) = 1.645(5), B(2)−N(51) = 1.644(5), B(2)−N(61) = 1.626(5), B(1)−C(11) = 1.607(5), B(2)−C(41) = 1.605(5), N(1)−Si(1) = 1.780(3); B(1)−N(1)−B(2) = 123.9(3), N(1)−B(1)−C(11) = 123.5(3), N(1)−B(2)−C(41) = 122.8(3), N(21)−B(1)−N(31) = 92.5(2), N(51)−B(2)−N(61) = 93.2(2), B(1)−N(1)−Si(1) = 118.6(2), B(2)−N(1)−Si(1) = 117.4(2); C(11)−B(1)−N(1)−B(2) = 11.1(5), C(41)−B(2)−N(1)−B(1) = 8.6(5), C(11)−B(1)−N(1)−Si(1) = −165.2(3); C(11)−C(15)//C(41)−C(45) = 11.3.

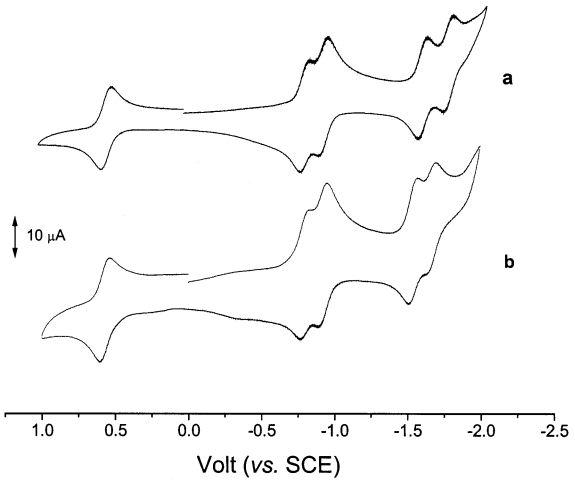

Figure 8. Cyclic voltammograms recorded at a platinum electrode on DMF solutions containing $[NEt_4](PF_6)$ (0.1 mol dm^{-3}) and (a) **[2](PF$_6$)$_2$** (0.6×10^{-3} mol dm^{-3}); (b) **[13](CO$_2$CF$_3$)$_2$** (0.6×10^{-3} mol dm^{-3}). Scan rate 0.2 V s^{-1}.

voltammetric behavior of complex **[2]**$^{2+}$ with that of **[13]**$^{2+}$ in *N*,*N*-dimethylformamide solution.

An analysis of the cyclic voltammograms of **[11]**$^{2+}$ and **[13]**$^{2+}$ with scan rates varying from 0.02 to 1.00 V s^{-1} confirms the chemical reversibility (i_{pc}/i_{pa} constantly equal to 1), as well as the electrochemical reversibility (ΔE_p constantly close to 60 mV) of all electron transi-

Table 2. Formal Electrode Potentials (V, vs SCE) and Peak-to-Peak Separations (mV, in parentheses) for the Redox Changes Exhibited by Complexes [2](PF$_6$)$_2$, [5](PF$_6$)$_2$, [7](PF$_6$)$_2$, [11](PF$_6$)$_2$, [12](PF$_6$)$_2$, and [13](CO$_2$CF$_3$)$_2$ in *N*,*N*-Dimethylformamide Solution Containing [NEt$_4$]PF$_6$ (0.1 mol dm^{-3}) as Supporting Electrolyte

	$E^{o\prime a}$ (V)			$E^{o\prime a}$ (V)			$E^{o\prime a}$ (V)		
	4+/3+	3+/2+	K_{com}	2+/+	+/0	K_{com}	0/−	−/2−	K_{com}
[2](PF$_6$)$_2$		+0.57 (*68*)		−0.80 (*63*)	−0.93 (*68*)	160	−1.55 (*56*)	−1.67 (*60*)	110
[5](PF$_6$)$_2$	+0.53 (*65*)	+0.47 (*60*)	10	−0.75 (*50*)	−0.88 (*60*)	160	−1.78 (*100*)	−1.96[b] -	1125
[7](PF$_6$)$_2$	+0.52[c] (*90*)		*d*	−0.65 (*30*)	−0.83 (*56*)	1125	−1.80[b]		*d*
[11](PF$_6$)$_2$		+0.51 (*64*)		−0.85 (*50*)	−1.02 (*55*)	760	−1.71 (*75*)	−1.83 (*65*)	110
[12](PF$_6$)$_2$		+0.55 (*120*)		−0.81 (*62*)	−0.94 (*50*)	160	−1.64 (*100*)	−1.80 (*100*)	515
[13](CO$_2$CF$_3$)$_2$		+0.53 (*70*)		−0.84 (*66*)	−0.96 (*70*)	110	−1.63 (*84*)	−1.83 (*58*)	2455
FcH	+0.49 (72)								

[a]Measured at 0.2 V s^{-1}. [b]Peak potential for irreversible process. [c]Two-electron process. [d]Not determinable by electrochemical measurements.

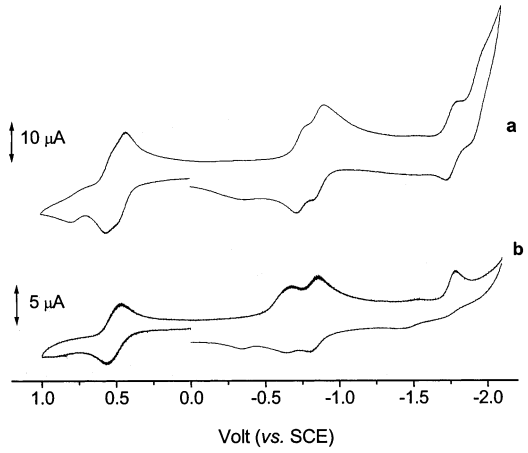

Figure 9. Cyclic voltammograms recorded at a platinum electrode on DMF solutions containing [NEt$_4$](PF$_6$) (0.1 mol dm^{-3}) and (a) **[5](PF$_6$)$_2$**; (b) **[7](PF$_6$)$_2$**. Scan rate 0.2 V s^{-1}.

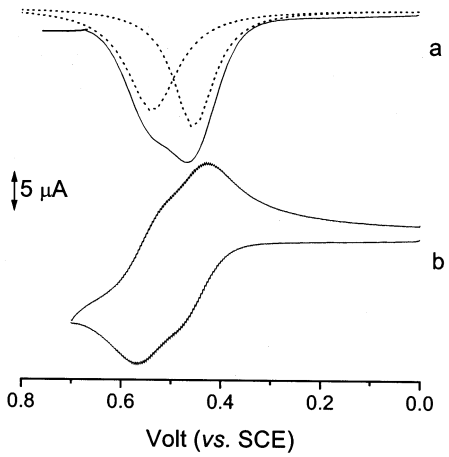

Figure 10. Osteryoung square wave (a) and cyclic (b) voltammograms recorded at a platinum electrode on a DMF solution containing [NEt$_4$](PF$_6$) (0.1 mol dm^{-3}) and **[5](PF$_6$)$_2$**. Scan rates: (a) 0.1 V s^{-1}; (b) 0.2 V s^{-1}.

tions involved. This suggests that no significant structural reorganization is caused by these redox processes. In the case of **[12]**$^{2+}$, both the oxidation (ΔE_p = 120 mV at a scan rate of 0.2 V s^{-1}) and the last couple of reductions (ΔE_p = 100 mV at a scan rate of 0.2 V s^{-1}) appear to be electrochemically quasi-reversible. As expected, controlled potential coulometric tests on **[11]**$^{2+}$−**[13]**$^{2+}$ performed in correspondence with the anodic step (E_w = +1.0 V) revealed the consumption of one electron *per* molecule. At variance with the chemical stability of **[2]**$^{3+}$, all the electrogenerated complexes **[11]**$^{3+}$−**[13]**$^{3+}$ tend to decompose slowly.

As illustrated in Figure 9, the cyclic voltammetric behavior of **[5]**$^{2+}$ and **[7]**$^{2+}$ is rather similar to that of the ferrocenophanes **[2]**$^{2+}$ and **[11]**$^{2+}$−**[13]**$^{2+}$. As the main difference, **[5]**$^{2+}$ exhibits two ferrocene-centered one-electron oxidations (Figure 10), while in complex **[7]**$^{2+}$ the ferrocene moieties are oxidized in a single two-electron step. As far as the reduction processes are concerned, the first split bipy-centered reduction wave is well evident in both cases, whereas for the second couple only the first reduction wave is clearly visible. The second reduction wave is probably masked by the solvent discharge. An analysis of the cyclic voltammograms of **[5]**$^{2+}$ with scan rates varying from 0.02 to 1.00 V s^{-1} confirms that the oxidation process as well as the first couple of reduction processes is chemically and electrochemically reversible. The width of the oxidation peak for **[7]**$^{2+}$ (ΔE_p = 90 mV at a scan rate of 0.2 V s^{-1}) is confidently ascribed to the unresolved overlapping of two one-electron removals. In the case of **[7]**$^{2+}$ the first two electron additions are partially chemically reversible, whereas further electron transfer is irreversible.

The formal electrode potentials of the above-discussed redox changes are compiled in Table 2. The oxidation potentials of **[5]**$^{2+}$, **[7]**$^{2+}$, and **[11]**$^{2+}$−**[13]**$^{2+}$ are slightly shifted to more positive values compared to parent ferrocene ($E^{o\prime}$ = +0.49 V), **[A]PF$_6$** (R = OEt: $E^{o\prime}$ = +0.43 V; R = N(CH$_2$)$_4$: $E^{o\prime}$ = +0.41 V),[5] and **[B](PF$_6$)$_2$** (R = Me: $E^{o\prime}$ = +0.43 V).[5] The average potential values of each reduction couple are also quite similar to the respective potentials of **[A]PF$_6$** (R = OEt: $E^{o\prime}$ = −0.88 V, −1.54 V; R = N(CH$_2$)$_4$: $E^{o\prime}$ = −0.99 V, −1.68 V)[5] and **[B](PF$_6$)$_2$** (R = Me: $E^{o\prime}$ = −0.98 V, −1.71 V).[5]

Moreover, the redox behavior of complexes **[5]**$^{2+}$, **[7]**$^{2+}$, and **[11]**$^{2+}$−**[13]**$^{2+}$ almost reproduces that previously reported for **[2]**$^{2+}$, one main difference being the higher stability of the electrogenerated species in the latter case. Values of the comproportionation constant K_{com} [K_{com} = exp(16.95 × ΔE)] of 160 and 110, respectively, allow us to classify **[2]**$^{+}$ and **[2]**$^{-}$ as partially delocalized (on the electrochemical time scale) Robin-Day class II systems. Most interestingly, the K_{com} data of **[5]**$^{2+}$, **[7]**$^{2+}$, and **[11]**$^{2+}$−**[13]**$^{2+}$ vary over a much wider range. For example, K_{com}(**[13]**$^{2+}$/**[13]**^{0}) = 110 is 1 order of magnitude smaller compared to K_{com}(**[13]**^{0}/**[13]**$^{2-}$) = 2455. The same is true for a comparison of the comproportionation constants of equivalent redox processes in different compounds (e.g., K_{com}(**[5]**$^{2+}$/**[5]**^{0})

= 160; K_{com}(**[7]**$^{2+}$/**7**^{0}) = 1125). On the basis of the data available, there is no obvious correlation between the nature of the bridging unit and the K_{com} values. This finding gives some insight into the mechanism of electronic communication within the molecules, since the nitrogen substituent in **[11]**$^{2+}$−**[13]**$^{2+}$, which is placed like a dielectric between two molecular capacitor plates, can be expected to have a major influence on the Coulomb interaction of charges delocalized over the two 2,2′-bipyridylboronium fragments. Nevertheless, identical K_{com} values are found for some complexes possessing very different bridging units {e.g., first reduction couple in **[2](PF$_6$)$_2$** and **[11](PF$_6$)$_2$**}, and on the other hand, rather different K_{com} values can be observed in the first and in the second reduction wave of the same compound {e.g., **[13](CO$_2$CF$_3$)$_2$**}. This suggests the electronic communication between the redox-active [Bbipy]$^+$ sites in **[2](PF$_6$)$_2$** and **[11](PF$_6$)$_2$**−**[13](CO$_2$CF$_3$)$_2$** to be transmitted mainly via a BXB *through-bond* rather than via a Coulombic *through-space* pathway [X = O, N(R)]. This interpretation is further supported by the fact that the degree of electronic interaction is not diminished in the structurally flexible complexes **[5](PF$_6$)$_2$** and **[7](PF$_6$)$_2$** compared to the rigid *ansa*-ferrocenes **[11](PF$_6$)$_2$**−**[13](CO$_2$CF$_3$)$_2$**, even though the dinuclear species are able to alleviate Coulomb repulsion by adopting a conformation in which the [Bbipy]$^+$ sites are further apart from each other. In addition, even the two ferrocene units in the symmetric complex **[5]**$^{2+}$ are oxidized at slightly different potentials, thereby testifying to a weak electronic interaction between them.

Conclusion

A series of multistep redox systems have been synthesized and characterized by cyclic voltammetry. Common to all compounds under investigation are 2,2′-bipyridylboronium {[Bbipy]$^+$} ions as key elements, which function as reversible two-electron acceptors. In the most rigid structures, two [Bbipy]$^+$ fragments are doubly bridged via their boron atoms by a 1,1′-ferrocenylene linker, on one hand, and an oxygen atom {**[2](PF$_6$)$_2$**} or an NR group, on the other {**[11](PF$_6$)$_2$**, R = 4-methoxyphenyl; **[12](PF$_6$)$_2$**, R = 4-bromophenyl; **[13](CO$_2$CF$_3$)$_2$**, R = trimethylsilyl}. In the conformationally more flexible species, two [Bbipy]$^+$ sites are connected by one oxygen atom {**[5](PF$_6$)$_2$**} or one C(H)CN group {**[7](PF$_6$)$_2$**} only. In addition, a ferrocenyl substituent is attached to each boron atom. In all species, the two [Bbipy]$^+$ acceptor units are symmetry-related. Nevertheless, four well-defined one-electron transfer processes rather than two two-electron waves are observed upon reduction in the cyclic voltammograms. This feature clearly indicates both electroactive units to be electronically communicating. The respective comproportionation constants are similar, for example, in the *ansa*-ferrocene **[2](PF$_6$)$_2$** and in the open-chain derivative **[5](PF$_6$)$_2$**. Moreover, complex 1,1′-fc[B(Me)bipy]$_2$, which possesses a ferrocenylene bridge only, exhibits no correlation between the two 2,2′-bipyridylboronium units at all. Consequently, a 1,1′-ferrocenylene linker does not appear to be a transmitter of electronic interaction, while an oxygen bridge or NR (R = 4-methoxyphenyl, 4-bromophenyl, trimethylsilyl) and C(H)CN groups are quite efficient in this respect. It should be noted that the distance between the midpoints of the C(22)−C(32) bond and the C(52)−C(62) bond is 6.73 Å in **[11](PF$_6$)$_2$**; similar values are observed for **[2](PF$_6$)$_2$** (6.47 Å) and **[13](CO$_2$CF$_3$)$_2$** (7.15 Å). A distance of 8.53 Å is found between the analogous bonds in the open-chain species 1,1′-fc[B(Me)bipy]$_2$. Given this background, the electronic communication between the [Bbipy]$^+$ fragments in the *ansa*-ferrocene derivatives should probably not be attributed to a mere Coulomb effect.

All complexes possess a deep blue-purple color attributable to charge-transfer interactions between the electron-rich ferrocenyl/1,1′-ferrocenylene substituents on one hand and the electron-poor 2,2′-bipyridylboronium ions on the other. In contrast, no evidence for additional charge transfer from the 4-methoxyphenyl substituent into the [Bbipy]$^+$ moieties is observed in the range λ = 190−1100 nm of the UV/vis spectrum of **[11](PF$_6$)$_2$**.

Experimental Section

General Considerations. All reactions and manipulations of air-sensitive compounds were carried out in dry, oxygen-free argon using standard Schlenk ware. Solvents were freshly distilled under argon from Na/benzophenone (toluene, hexane, pentane) or passed through a 4 Å molecular sieves column (CH_2Cl_2, acetonitrile) prior to use; NEt_3 was freshly distilled under argon from CaH_2. **[1]Br$_2$**, **[4]Br**, and **9** were prepared as described in the literature.[5,11] NMR: Bruker AMX 250, AMX 400, Bruker DPX 250. ^{11}B and ^{19}F NMR spectra were reported relative to external $BF_3{\cdot}Et_2O$ and $CFCl_3$, respectively. ^{29}Si NMR spectra were recorded using the INEPT pulse sequence with empirically optimized parameters for polarization transfer from the methyl substituents. Unless stated otherwise, all NMR spectra were run at ambient temperature. Abbreviations: s = singlet; d = doublet; tr = triplet; vtr = virtual triplet; br = broad; m = multiplet; n.r. = multiplet expected in the ^{1}H NMR spectrum but not resolved; n.o. = signal not observed; ar = aryl ring of the 4-methoxyphenyl or the 4-bromophenyl substituent; 2,2′-bipy = 2,2′-bipyridine. UV−vis spectra were recorded on a Varian Cary 50 UV−visible spectrophotometer. HPLC: Reprosil AQ column and RI-Detection. Elemental analyses: Microanalytical Laboratory of the Frankfurt University.

Synthesis of [3](PF$_6$)$_2$. [1]Br$_2$ (0.89 g, 1.06 mmol) in 30 mL of acetonitrile was treated at ambient temperature with an excess of H_2O (0.1 g, 5.56 mmol) and neat Et_3N (0.32 g, 3.16 mmol). The mixture was stirred for 6 h, whereupon it gradually changed its color from blue to red-purple, and a deep red-purple precipitate formed. After the mother liquor had been removed by filtration, the solid residue was dried in vacuo, dissolved in 10 mL of water, and added dropwise with stirring to an aqueous solution of NH_4PF_6 (0.59 g, 3.62 mmol), whereupon **[3](PF$_6$)$_2$** precipitated quantitatively. The precipitate was collected on a frit and triturated with diethyl ether (10 mL). Deep red-purple X-ray quality crystals were grown by gas-phase diffusion of diethyl ether into an acetonitrile solution of **[3](PF$_6$)$_2$**. Yield: 0.69 g (77%).

^{11}B NMR (128.4 MHz, CD_3CN): δ 12.8 ($h_{1/2}$ = 280 Hz). ^{1}H NMR (250.1 MHz, CD_3CN): δ 4.07, 4.30 (2 × vtr, 2 × 4H, J = 1.8 Hz, C_5H_4), 5.20 (s, 2H, OH), 8.15 (ddd, 4H, J = 5.6, 5.6, 3.4 Hz, bipy-5,5′), 8.62 (m, 8H, bipy-4,4′ and bipy-3,3′), 9.10 (dtr, 4H, J = 5.6, 1.1 Hz, bipy-6,6′). ^{13}C NMR (62.9 MHz, CD_3CN): δ 71.0, 72.6, (C_5H_4), n.o. (C_5H_4-*ipso*), 123.7 (bipy-3,3′), 130.0 (bipy-5,5′), 144.5 (bipy-6,6′), 145.3 (bipy-2,2′), 146.5 (bipy-4,4′). UV−vis in acetonitrile: λ (nm) 521 (1700), 314 (34700), 303 (34900). ESI-MS of **[3](PF$_6$)$_2$**: m/z 697 [M − PF_6]$^+$, 276 [M − 2PF_6]$^{2+}$. Anal. Calcd for $C_{30}H_{26}B_2F_{12}FeN_4O_2P_2$ [841.96] C, 42.80; H, 3.11; N, 6.65. Found: C, 42.38; H, 3.28; N, 6.65.

Synthesis of [5](PF$_6$)$_2$. An excess of neat Et_3N (0.24 g, 2.37 mmol) was added at ambient temperature to **[4]Br** (0.40 g, 0.78 mmol) in acetonitrile (10 mL; commercially available acetonitrile was used as purchased without drying; no additional water was required). While the mixture was stirred at ambient temperature for 2 days, it gradually changed its color from deep blue to purple. After filtration from a small amount of insoluble material and evaporation of the filtrate in vacuo, a deep purple solid was obtained. The crude material was treated with 5 mL of water, and the resulting clear purple solution added dropwise with stirring to an aqueous solution of NH_4PF_6 (0.14 g, 0.86 mmol), whereupon **[5](PF$_6$)$_2$** precipitated quantitatively. The precipitate was collected on a frit and triturated with diethyl ether (10 mL). Deep purple X-ray quality crystals were grown by gas-phase diffusion of diethyl ether into an acetonitrile solution of **[5](PF$_6$)$_2$**. Yield: 0.22 g (56%).

^{11}B NMR (128.4 MHz, CD_3CN): δ 9.2 ($h_{1/2}$ = 230 Hz). ^{1}H NMR (250.1 MHz, CD_3CN): δ 3.52 (s, 10H, C_5H_5), 3.60, 4.06 (2 × vtr, 2 × 4H, J = 1.8 Hz, C_5H_4), 8.09 (m, 4H, bipy-5,5′), 8.61 (m, 8H, bipy-3,3′,4,4′), 8.71 (d, 4H, J = 5.6 Hz, bipy-6,6′). ^{13}C NMR (62.9 MHz, CD_3CN): δ 69.0 (br, C_5H_5), 71.3, 71.4 (2 × br, C_5H_4), n.o. (C_5H_4-*ipso*), 124.0 (bipy-3,3′), 130.3 (bipy-5,5′), 144.3 (bipy-6,6′), 145.2 (bipy-2,2′), 146.7 (bipy-4,4′). UV−vis in acetonitrile: λ (nm) 552, 315, 303. ESI-MS of **[5](PF$_6$)$_2$**: *m*/*z* 865 [M − PF_6]$^+$. Anal. Calcd for $C_{40}H_{34}B_2F_{12}Fe_2N_4OP_2$ [1009.97]: C, 47.57; H, 3.39; N, 5.55. Found: C, 47.84; H, 3.72; N, 5.86.

Synthesis of [6]PF$_6$ and [7](PF$_6$)$_2$. An excess of neat Et_3N (1.60 g, 15.81 mmol) was added at ambient temperature to **[4]Br** (2.70 g, 5.28 mmol) in 40 mL of carefully dried acetonitrile. The solution was stirred for 2 days, while its color gradually changed from deep blue to brown, and a small amount of precipitate formed. After filtration, the filtrate was evaporated to dryness in vacuo to yield a deep brown solid material. The crude product was treated with 20 mL of water, and the resulting clear brown solution added dropwise with stirring to an aqueous solution of NH_4PF_6 (0.95 g 5.83 mmol), whereupon **[6]PF$_6$** and **[7](PF$_6$)$_2$** precipitated quantitatively. The precipitate was collected on a frit and triturated with diethyl ether (20 mL). **[6]PF$_6$** and **[7](PF$_6$)$_2$** were separated by repeated crystallization from a mixture of acetonitrile and diethyl ether, in which **[7](PF$_6$)$_2$** possesses the lower solubility. Deep brown X-ray quality crystals of **[7](PF$_6$)$_2$** were grown by gas-phase diffusion of diethyl ether into an acetonitrile solution of **[7](PF$_6$)$_2$**. Yield of **[6]PF$_6$**: 2.08 g (73%). Yield of **[7](PF$_6$)$_2$**: 0.43 g, (16%).

[6]PF$_6$. ^{11}B NMR (128.4 MHz, CD_3CN): δ 6.1 ($h_{1/2}$ = 170 Hz). ^{1}H NMR (250.1 MHz, CD_3CN): δ 2.39 (s, 2H, BCH_2), 3.99 (n.r., 2H, C_5H_4), 4.12 (s, 5H, C_5H_5), 4.33 (n.r., 2H, C_5H_4), 8.19 (ddd, 2H, J = 7.3, 5.9, 1.5 Hz, bipy-5,5′), 8.71 (m, 4H, bipy-3,3′,4,4′), 9.05 (d, 2H, J = 5.9 Hz, bipy-6,6′). ^{13}C NMR (62.9 MHz, CD_3CN): δ 10.7 (br, BCH_2), 69.3 (C_5H_5), 71.2, 71.2, (C_5H_4), n.o. (C_5H_4-*ipso*), 120.6 (CN), 123.9 (bipy-3,3′), 129.9 (bipy-5,5′), 144.2 (bipy-6,6′), 146.0 (bipy-2,2′), 146.3 (bipy-4,4′). ESI-MS of **[6]PF$_6$**: *m*/*z* 392 [M − PF_6]$^+$. Anal. Calcd for $C_{22}H_{19}BF_6FeN_3P$ [537.03]: C, 49.20; H, 3.57; N, 7.82. Found: C, 49.22; H, 3.74; N, 7.89.

[7](PF$_6$)$_2$. ^{11}B NMR (128.4 MHz, CD_3CN): δ 6.4 ($h_{1/2}$ = 270 Hz). ^{1}H NMR (250.1 MHz, CD_3CN): δ 2.52 (s, 1H, BCH), 3.37 (s, 10H, C_5H_5), 3.87 (n.r., 4H, C_5H_4), 4.20, 4.21 (2 × n.r., 2 × 2H, C_5H_4), 7.89 (ddd, 2H, J = 7.3, 5.8, 1.6 Hz, bipy-5,5′), 8.09 (ddd, 2H, J = 5.5, 5.5, 3.7 Hz, bipy-5,5′). 8.29 (d, 2H, J = 5.6 Hz, bipy-6,6′), 8.64 (m, 8H, bipy-3,3′,4,4′), 8.89 (d, J = 5.7 Hz, 2H, bipy-6,6′). ^{13}C NMR (100.6 MHz, CD_3CN): δ 15.6 (CH), 68.9 (C_5H_5), 71.0, 71.5, 71.7, 71.8 (C_5H_4), n.o. (C_5H_4-*ipso*), 124.3 (CN), 124.5, 124.7 (bipy-3,3′), 130.2, 130.6 (bipy-5,5′), 144.5, 144.8 (bipy-6,6′), 145.6, 145.7 (bipy-2,2′), 146.7, 147.0 (bipy-4,4′). UV−vis in acetonitrile: λ (nm) 314, 313, 273. ESI-MS of **[7](PF$_6$)$_2$**: *m*/*z* 888 [M − PF_6]$^+$, 371 [M − 2PF_6]$^{2+}$. Anal. Calcd for $C_{42}H_{35}B_2F_{12}Fe_2N_5P_2$ [1033.01]: C, 48.83; H, 3.42; N, 6.78. Found: C, 48.73; H, 3.29; N, 6.75.

Synthesis of [8](PF$_6$)$_2$. A CH_2Cl_2 (20 mL) solution of 4-methoxyaniline (0.28 g, 2.27 mmol) was added dropwise with stirring at 0 °C to **[1]Br$_2$** (0.47 g, 0.56 mmol) in 50 mL of CH_2Cl_2. The color of the reaction mixture changed from blue to purple, and a pale brown precipitate formed. The resulting slurry was allowed to warm to ambient temperature and stirred for 6 h. After all insolubles had been removed by filtration, the filtrate was evaporated in vacuo to yield a red-purple solid. The crude material was dissolved in 10 mL of water, and the resulting solution added dropwise with stirring to an aqueous solution of NH_4PF_6 (0.20 g, 1.23 mmol), whereupon **[8](PF$_6$)$_2$** precipitated quantitatively. Deep red-purple X-ray quality crystals of **[8](PF$_6$)$_2$** were grown by gas-phase diffusion of diethyl ether into an acetonitrile solution of **[8](PF$_6$)$_2$**. Yield: 0.48 g (81%).

^{11}B NMR (128.3 MHz, CD_3CN): δ 7.4 ($h_{1/2}$ = 450 Hz). ^{1}H NMR (250.1 MHz, CD_3CN): δ 3.57 (s, 6H, 2 × OCH_3), 3.87, 4.17 (2 × vtr, 2 × 4H, J = 1.8 Hz, C_5H_4), 5.96, 6.47 (2 × dd, 2 × 4H, J = 6.6, 2.3 Hz, ar-2,3,5,6), 8.11 (ddd, 4H, J = 7.6, 5.6, 1.2 Hz, bipy-5,5′), 8.73 (ddd, 4H, J = 7.6, 7.6, 1.4 Hz, bipy-4,4′), 8.95 (m, 8H, bipy-3,3′,6,6′). ^{13}C NMR (62.9 MHz, CD_3CN): δ 55.6 (OCH_3), 70.8, 71.5 (C_5H_4), n.o. (C_5H_4-*ipso*), 115.3, 116.7 (ar-2,3,5,6), 124.8 (bipy-3,3′), 129.8 (bipy-5,5′), 140.6 (ar-*C*N), 144.1 (bipy-6,6′), 145.2 (bipy-2,2′), 146.4 (bipy-4,4′), 152.7 (ar-*C*O). UV−vis in acetonitrile: λ (nm) 522, 314, 304, 244. ESI-MS of **[8](PF$_6$)$_2$**: *m*/*z* 381 (M − 2PF_6)$^{2+}$. Anal. Calcd for $C_{44}H_{40}B_2F_{12}FeN_6O_2P_2$ [1052.23]: C, 50.22; H, 3.83; N, 7.99. Found: C, 50.62; H, 3.84; N, 8.24.

Synthesis of 10. Compound **9** (1.23 g, 2.34 mmol) in 40 mL of toluene was treated at −78 °C with a mixture of 4-methoxyaniline (0.29 g, 2.35 mmol) and Et_3N (0.47 g, 4.64 mmol) in 20 mL of toluene. The color of the reaction mixture changed gradually from red to yellow, and a pale yellow precipitate formed upon warming to ambient temperature. The resulting slurry was stirred for 1 h and then heated at reflux temperature for 2 h. After all insolubles had been removed by filtration, the filtrate was condensed to a volume of about 10 mL in vacuo and stored at −30 °C overnight. The yellow crystalline precipitate obtained was isolated by filtration, triturated with cold hexane (5 mL), and dried in vacuo. Yield: 0.69 g (61%).

^{11}B NMR (128.4 MHz, $CDCl_3$): δ 46.3 ($h_{1/2}$ = 550 Hz). ^{1}H NMR (250.1 MHz, $CDCl_3$): δ 3.86 (s, 3H, OCH_3), 4.41, 4.67 (2 × vtr, 2 × 4H, J = 1.7 Hz, C_5H_4), 6.95, 7.12 (2 × dd, 2 × 2H, J = 6.7, 2.2 Hz, ar-2,3,5,6). ^{13}C NMR (62.9 MHz, $CDCl_3$): δ 55.3 (OCH_3), 76.9, 78.3 (C_5H_4), n.o. (C_5H_4-*ipso*), 114.0, 129.1 (ar-2,3,5,6), 139.3 (ar-*C*N), 157.9 (ar-*C*O).

Synthesis of [11](PF$_6$)$_2$. 2,2′-Bipyridine (0.30 g, 1.92 mmol) in 10 mL of toluene was added with stirring at −78 °C to **10** (0.46 g, 0.95 mmol) in 40 mL of toluene. The mixture instantaneously adopted a deep blue color, and a blue precipitate gradually formed upon warming to ambient temperature. The slurry was stirred for 5 h, and the blue solid of **[11]Br$_2$** was collected on a frit, triturated with toluene (3 × 10 mL), and dried in vacuo. $TlPF_6$ (0.67 g, 1.92 mmol) in 20 mL of acetonitrile was added to a slurry of **[11]Br$_2$** in acetonitrile (20 mL) at ambient temperature. A blue solution and a colorless precipitate (TlBr) was obtained. The slurry was stirred for 1 h and filtered, and the volume of the filtrate was reduced to about 10 mL in vacuo. Deep purple X-ray quality crystals were grown by gas-phase diffusion of diethyl ether into an acetonitrile solution of **[11](PF$_6$)$_2$**. Yield: 0.81 g (92%).

^{11}B NMR (128.3 MHz, CD_3CN): δ 10.0 ($h_{1/2}$ = 300 Hz). ^{1}H NMR (250.1 MHz, CD_3CN): δ 3.28 (s, 3H, OCH_3), 4.31, 4.45 (2 × vtr, 2 × 4H, J = 1.5 Hz, C_5H_4), 5.50, 5.90 (2 × dd, 2 × 2H, J = 6.7, 2.3 Hz, ar-2,3,5,6), 8.25 (m, 8H, bipy-3,3′,5,5′), 8.50 (ddd, 4H, J = 7.9, 7.9, 1.3 Hz, bipy-4,4′), 9.51 (d, 4H, J = 5.7 Hz, bipy-6,6′). ^{13}C NMR (60.0 MHz, CD_3CN): δ 55.5 (OCH_3), 72.9, 73.2 (C_5H_4), n.o. (C_5H_4-*ipso*), 114.8 (ar-3,5 or 2,6), 123.7 (bipy-3,3′), 130.3 (bipy-5,5′), 130.8 (ar-2,6 or 3,5), 138.6 (ar-*C*N), 145.2, 145.3, 146.2 (bipy-2,2′,4,4′,6,6′), 156.9 (ar-*C*O).

UV−vis in acetonitrile: λ (nm) 539, 315, 304, 244. ESI-MS of **[11](PF$_6$)$_2$**: *m*/*z* 784 [M − PF$_6$]$^+$. Anal. Calcd for $C_{37}H_{31}B_2F_{12}FeN_5OP_2$ [929.08]: C, 47.83; H, 3.36; N, 7.54. Found: C, 47.44; H, 3.75; N, 7.44.

Synthesis of [12](PF$_6$)$_2$. 4-Bromo-*N*,*N*-bis(trimethylsilyl)-aniline (0.61 g, 1.93 mmol) in 40 mL of toluene was added with stirring to **9** (1.02 g, 1.94 mmol) in 120 mL of toluene at −78 °C. The reaction mixture was allowed to warm to ambient temperature and then heated under reflux for about 2.5 h, whereupon the color changed gradually from yellow to red and a small amount of yellow precipitate formed. The slurry was cooled to ambient temperature again and filtered, and the volume of the filtrate was reduced to about 15 mL in vacuo. The yellow crystalline solid, which formed upon storage of this solution at −30 °C overnight, was isolated by filtration, triturated with cold hexane (2 × 2 mL), and redissolved in about 40 mL of toluene. Addition of 2,2′-bipyridine (0.61 g, 3.91 mmol) in toluene (20 mL) at −78 °C resulted in an instantaneous color change from yellow to deep blue and the formation of a deep blue precipitate. The slurry was stirred for 1 h at ambient temperature, and the blue solid of **[12]Br$_2$** was collected on a frit, triturated with toluene (3 × 10 mL), and dried in vacuo. TlPF$_6$ (0.77 g, 2.20 mmol) in 10 mL of acetonitrile was added at ambient temperature to a slurry of **[12]Br$_2$** (0.93 g, 1.10 mmol) in 10 mL of acetonitrile. After stirring for 1 h, TlBr was filtered off, and the volume of the filtrate was reduced to about 15 mL in vacuo. Deep purple X-ray quality crystals were grown by gas-phase diffusion of diethyl ether into an acetonitrile solution of **[12](PF$_6$)$_2$**. Yield: 1.00 g (53%).

^{11}B NMR (128.3 MHz, CD_3CN): δ 10.1 ($h_{1/2}$ = 730 Hz). ^{1}H NMR (250.1 MHz, $CDCl_3$): δ 4.32, 4.44 (2 × vtr, 2 × 4H, J = 1.7 Hz, C_5H_4), 5.55, 6.54 (2 × dd, 2 × 2H, J = 6.3, 2.1 Hz, ar-2,3,5,6), 8.25 (ddd, 4H, J = 7.6, 5.8, 1.5 Hz, bipy-5,5′), 8.33 (d, 4H, J = 7.6 Hz, bipy-3,3′), 8.53 (ddd, 4H, J = 7.6, 7.6, 1.7 Hz, bipy-4,4′), 9.51 (d, 4H, J = 5.8 Hz, bipy-6,6′). ^{13}C NMR (62.9 MHz, CD_3CN): δ 72.9, 73.1 (C_5H_4), n.o. (C_5H_4-*ipso*), 121.1 (ar-*C*Br), 123.9 (bipy-3,3′), 130.4 (bipy-5,5′), 132.0, 132.8 (ar-2,3,5,6), 145.1 (bipy-2,2′), 145.3 (bipy-4,4′ or 6,6′), 145.8 (ar-*C*N), 146.3 (bipy-4,4′ or 6,6′). UV−vis in acetonitrile: λ (nm) 531, 317, 305. ESI-MS of **[12](PF$_6$)$_2$**: *m*/*z* 832 [M − PF$_6$]$^+$, 343 [M − 2PF$_6$]$^{2+}$. Anal. Calcd for $C_{36}H_{28}B_2BrF_{12}FeN_5P_2$ [977.95]: C, 44.21; H, 2.89; N, 7.16. Found: C, 44.07; H, 2.79; N, 6.96.

Synthesis of [13](CO$_2$CF$_3$)$_2$. A clear colorless toluene solution (30 mL) of lithium bis(trimethylsilyl)amide (0.84 g, 5.02 mmol) was added dropwise with stirring at −78 °C to **9** (2.64 g, 5.03 mmol) in 30 mL of toluene. The resulting deep red solution was allowed to warm to ambient temperature, heated at 90 °C for 2 h, and then cooled to −78 °C again. 2,2′-Bipyridine (1.60 g, 10.24 mmol) in 30 mL of toluene was added, whereupon the color of the reaction mixture changed instantaneously from deep red to deep blue, and a blue precipitate formed. The deep blue slurry was stirred at ambient temperature for 10 h. The solid material was isolated by filtration, triturated with toluene (3 × 10 mL), and dried in vacuo. An analytically pure sample was obtained by HPLC separation using (H_2O/0.1% trifluoroacetic acid)/acetonitrile, 70:30, as eluent. Deep blue-purple X-ray quality crystals were grown by gas-phase diffusion of diethyl ether into an acetonitrile solution of **[13](CO$_2$CF$_3$)$_2$**. Yield: 1.67 g (40%).

^{11}B NMR (128.4 MHz, CD_3CN): δ 13.5 ($h_{1/2}$ = 250 Hz). ^{19}F NMR (235.3 MHz, CD_3CN): δ 2.06. ^{29}Si{^{1}H} NMR (49.7 MHz, CD_3CN): δ 5.62 (s, $SiMe_3$). ^{1}H NMR (400.1 MHz, $CDCl_3$): δ −1.02 (s, 9H, $SiMe_3$), 3.89, 4.02 (2 × vtr, 2 × 4H, J = 1.8 Hz, C_5H_4), 8.38 (ddd, 4H, J = 7.3, 5.7, 1.8 Hz, bipy-5,5′), 8.70 (m, 8H, bipy-3,3′,4,4′), 9.73 (dd, 4H, J = 5.7, 1.0 Hz, bipy-6,6′). ^{13}C NMR (62.9 MHz, CD_3CN): δ 2.9 ($SiMe_3$), 70.7, 71.5 (C_5H_4), n.o. (C_5H_4-*ipso*), 123.6 (bipy-3,3′), 129.3 (bipy-5,5′), 143.9 (bipy-2,2′), 145.0, 145.3 (bipy-4,4′,6,6′). UV−vis in acetonitrile: λ (nm) 547, 314, 304. ESI-MS of **[13](CO$_2$CF$_3$)$_2$**: *m*/*z* 303 [M − 2CO_2CF_3]$^{2+}$. Anal. Calcd for $C_{37}H_{33}B_2F_6FeN_5O_4Si$ [831.24] + 1.5 H_2O [27.03]: C, 51.78; H, 4.23; N, 8.16. Found: C, 51.91; H, 4.51; N, 7.82.

X-ray Single-Crystal Structure Determinations. Data collection was performed with graphite-monochromated Mo Kα radiation (λ = 0.71073) on a Siemens CCD three-circle diffractometer {**[3](PF$_6$)$_2$**, **[5](PF$_6$)$_2$**, **[8](PF$_6$)$_2$**, **[13](CO$_2$CF$_3$)$_2$**} and on a Stoe-IPDS-II two-circle-diffractometer {**[7](PF$_6$)$_2$**, **[11](PF$_6$)$_2$**}. The structures were solved with direct methods[13] and refined by full-matrix least-squares calculations on F^2 using the program SHELXL97.[14] Hydrogen atoms in **[3](PF$_6$)$_2$**, **[5](PF$_6$)$_2$**, **[7](PF$_6$)$_2$**, **[11](PF$_6$)$_2$**, and **[13](CO$_2$CF$_3$)$_2$** were placed in ideal positions and refined with fixed isotropic displacement parameters (riding model). For **[8](PF$_6$)$_2$**, the hydrogen atoms were taken from a difference Fourier synthesis and refined with isotropic thermal parameters. The crystal structure of **[7](PF$_6$)$_2$** contains disordered diethyl ether solvent molecules located in channels along the crystallographic *b*-axis. The atoms of one of these molecules could be located on discrete positions with the O atom on a center of inversion and with two different sites for the methylene groups. However, the second ether molecule could not be identified unambiguously, because six peaks were found for the five non-hydrogen atoms. From an inspection of the crystal packing it is evident that the second ether molecule is disordered along the lattice channel as well. The crystal of **[11](PF$_6$)$_2$** contains two ordered acetonitrile molecules and one ordered diethyl ether molecule in the unit cell.

Electrochemical Measurements. Materials and apparatus for electrochemistry have been described elsewhere.[15] All potential values are referred to the saturated calomel electrode (SCE).

Acknowledgment. M.W. gratefully acknowledges the financial support of the "Deutsche Forschungsgemeinschaft" (DFG). P.Z. gratefully acknowledges the financial support of the University of Siena (PAR 2001).

Supporting Information Available: Tables of structure refinement, atomic coordinates, bond lengths and angles, anisotropic displacement parameters, and hydrogen coordinates for complexes **[3](PF$_6$)$_2$**, **[5](PF$_6$)$_2$**, **[7](PF$_6$)$_2$**, **[8](PF$_6$)$_2$**, **[11](PF$_6$)$_2$**, and **[13](CO$_2$CF$_3$)$_2$**. This material is available free of charge via the Internet at http://pubs.acs.org.

OM020284R

(13) Sheldrick, G. M. *Acta Crystallogr.* **1990**, *A46*, 467.
(14) Sheldrick, G. M. *SHELXL-97. A Program for the Refinement of Crystal Structures*; Universität Göttingen, 1997.
(15) Bianchini, C.; Laschi, F.; Masi, D.; Ottaviani, F. M.; Pastor, A.; Peruzzini, M.; Zanello, P.; Zanobini, F. *J. Am. Chem. Soc.* **1993**, *115*, 2723.